Rare Metal Materials and Engineering
Volume 53, Issue 9, September 2024
Available online at www.rmme.ac.cn

Science Press

Cite this article as: Gu Bin, Xiong Zhihao, Yang Ping, et al. Microstructure Evolution and Deformation Behavior of Metastable β-Titanium Alloy Ti55511 in Die Forging[J]. Rare Metal Materials and Engineering, 2024, 53(09): 2420-2429. DOI: 10.12442/j.issn.1002-185X.20240152.

ARTICLE

Microstructure Evolution and Deformation Behavior of Metastable β-Titanium Alloy Ti55511 in Die Forging

Gu Bin[1], Xiong Zhihao[1], Yang Ping[1], Gu Xinfu[1], Yan Mengqi[2], Sha Aixue[2]

[1] School of Materials Science and Engineering, University of Science and Technology Beijing, Beijing 100083, China; [2] AECC Beijing Institute of Aeronautical Materials, Beijing 100095, China

Abstract: The effect of die forging on the microstructure evolution and deformation behavior of metastable β-titanium alloy Ti55511 was investigated by electron backscatter diffraction. Before die forging, the alloy Ti55511 was subjected to multi-pass forging to optimize the microstructural heterogeneity (texture) which can cause mechanical behavior anisotropy of titanium alloys. Results show that after die forging, Ti55511 components exhibit different microstructures and textures in different local areas. No <100> fiber texture is found in all areas with different degrees of deformation. Dynamic recrystallization occurs in the area where large strain occurs during the early stage of die forging. Basket-weave microstructure forms in most local areas.

Key words: metastable β-titanium alloy; microstructure; texture; die forging; EBSD

Among large-sized structural materials used in aerospace, metastable β-titanium alloys are very important because of their excellent properties such as strength and toughness[1–6]. For large-sized industrial component, mechanical properties of all different local areas should meet the industrial requirement, which are strongly related to texture and microstructure[7–13]. However, the inhomogeneity of microstructure and texture exists frequently in the center and edge of large-sized metastable β-titanium alloy after hot deformation, which leads to fluctuations of mechanical properties. In particular, for metastable β-titanium alloy with bimodal microstructure, it is very difficult to get homogenous microstructure, because the change of the grain size, shape, texture of α phase and degree of work hardening during every step of productions all can make microstructure inhomogeneous.

In order to obtain homogenous microstructure, avoid mechanical behavior anisotropy and obtain resulting good mechanical properties, metastable titanium alloys were usually subjected to complicated processing methods such as forging process, die forging and different thermal processes[1,14–18].

Moreover, it is well known that titanium alloys are sensitive to processing parameters[19–25]. There are many studies on the effect of deformation parameters on metastable titanium alloys during different deformation modes. In particular, for hot compression experiments, it is usually considered to simulate the forging process. In hot compression experiments, the effect of strain, strain rate and deformation temperature on the deformation behavior of metastable titanium alloys has been studied[26–30]. The <001> and <111> fiber textures form during hot compression, and the formation and evolution of these textures can be affected by deformation temperature, strain and strain rate. When deformed near β-transus temperature, the deformation behavior of β phase changes much due to the dynamic globalization of α phase[27,31].

With regard to the change of strain path, the deformation behavior of metastable titanium alloys during bar-rolling process was investigated[4]. In bar-rolling process, the deformation texture consisting of α- and γ-fiber components changes to a strong cube texture during recrystallization of β phase, which yields anisotropy and causes plastically soft behavior of the alloy due to the low Taylor factor[4]. The texture components include {001}<100>, α-fiber ranging from {100}<110> to {111}<110> and part of γ-fiber. It is also found that *c*-axis of equaixed α phase is perpendicular to the

Received date: March 15, 2024
Foundation item: National Science and Technology Project of China (JPPT-135-GH-2-017); Fellowship of China Postdoctoral Science Foundation (2022M720399)
Corresponding author: Gu Xinfu, Ph. D., Associate Professor, School of Materials Science and Engineering, University of Science and Technology Beijing, Beijing 100083, P. R. China, E-mail: xinfugu@ustb.edu.cn

rolling direction, which does not meet the Burgers orientation relationship. And some dynamic recrystallization (DRX) of β phase is facilitated by α phase. During hot deformation of metastable β-titanium alloys, the microstructure and mechanical behavior are related to DRX[32–35].

These studies contribute much to the understanding of microstructure evolution and deformation behavior of metastable titanium alloys. However, the studies on metastable β-titanium alloys are mostly focused on small samples of laboratory scale but not the engineering scale. There is very restricted research on this kind of alloy of engineering scale. For metastable β-titanium alloys, the production of industrial components is divided into two steps: firstly, forging 10–18 steps or more in β phase field and α+β phase field; secondly, die forging.

In our previous study, the evolution of microstructure and texture of metastable β-titanium alloy Ti55511 with engineering scale during the forging process, including alternate upsetting and stretching, has been investigated. It is found that microstructure and texture change much from the center to the edge after different forging passes. The volume fraction of α phase increases from the center to the edge of the sample with decreasing the forging temperature. The textures of the sample after forging are characterized by <110> and <111> fibers. The volume fraction of texture component changes much with the forging pass from the center to the edge of the large-sized sample.

Besides the forging processes, die forging of metastable β-titanium alloys with engineering scale is also important, because the industrial components after die forging directly determine the performance in service. Once failure of industrial components occurs during service process, the consequences will be serious. It is very essential to study the evolution of microstructure of metastable β-titanium alloys during service process. While the investigations on deformation behavior of metastable titanium alloys with engineering scale during die forging are still very rare.

In this study, the die forging process was applied on Ti55511 titanium alloy, before which the alloy had underwent multi-pass forging processes, and then the deformation behavior during die forging process and microstructure characteristics of different local areas were studied. The specific attention was paid to the following items: (1) basic microstructural characteristics under different strains in Ti55511 industrial components after die forging; (2) the differences in microstructure and texture between different local areas of Ti55511 industrial components after die forging; (3) the causes for significant microstructural differences[29–30].

1 Experiment

Ti55511 (Ti-5Al-5Mo-5V-1Cr-1Fe, wt%) is a metastable titanium alloy used in this study, with β-transus temperature (T_β) about 875 °C. Before die forging, Ti55511 titanium alloy bar was forged 10 passes by a 20 MN rapid forging machine. Each forging pass includes upsetting and stretching. Four passes were applied in the β phase field, and six passes were applied in α + β phase field. After ten passes, bimodal microstructure, consisting of equiaxed primary α phase and secondary α phase, forms in the center and at the edge of the bar.

The billet with size of 250 mm×350 mm×750 mm for die forging was obtained through compressing Ti55511 bar along radial direction, as shown in Fig. 1. Then, the billet was subjected to die forging process in specific dies including four steps. The first three die forging steps were applied at about 870 °C, and the last forging step was conducted at about 885 °C. After the last forging step, the Ti55511 component was annealed in α+β phase field. Fig. 1 shows the Ti55511 component before and after die forging and local areas for investigation. These areas were marked as area 1-1, area 1-2, area 1-3, area 2-1, area 2-2, area 3-1, area 3-2 and area 3-3. Because the component underwent different degrees of deformation during die forging, it had different thicknesses at different positions. The thickness was 20.0 mm for local area 1-1, 1-2 and 1-3, 4.4 mm for local area 2-1 and 2-2, and 10.6 mm for local area 3-1, 3-2 and 3-3.

According to calculations, area 1-1, 1-2 and 1-3 were referred as the area with small deformation under engineering strain of 20.0% (in the following just called strain), area 2-2 and 2-1 were referred as the area with large deformation under strain of 82.4%, and area 3-1, 3-2 and 3-3 were referred as the area with moderate deformation under strain of 57.6%.

The microstructure was characterized by Imager M2M optical microscope (OM) and TESCAN VGA3 scanning electron microscope (SEM) equipped with electron backscatter diffractometer (EBSD). The investigated surfaces were ground by 400#, 800#, 1200#, 2000# and 3000# SiC papers. Then, the samples were electropolished with the agent consisting of 5% perchloric acid+95% alcohol, and corroded in corrosive agent consisting of 3% hydrofluoric acid+7% nitric acid+90% water for 5 s. To scan a large area during EBSD experiments, the step size was set as 5 μm, whereas the step size was set to 80 nm for local areas. Orientation imaging microscopy (OIM) software was used to deal with the EBSD data. To test the texture of the β phase accurately and to observe the microstructure of the β phase clearly, the T-inverse

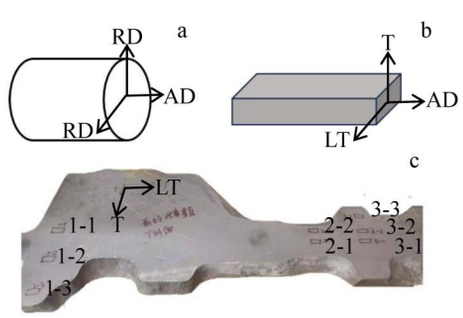

Fig.1 Schematics of Ti55511 bar after 10 passes of forging (a) and billet for die forging compressed from the Ti55511 bar (b); Ti55511 component after die forging (c) (T is compressing direction during die forging)

pole figure (T-IPF) map of β phase was presented by EBSD with removing α phase data. By checking the grain orientation spread (GOS), the recrystallized grains were picked out when GOS value was below 2°[36–38]. It is considered that GOS is related to distribution of strain and stored energy within a grain. A high value of GOS means a relatively high dislocation density and stored energy of deformed grain and vice versa.

2 Results and Discussion

2.1 Characteristics of microstructure and texture

It is well known that the metastable β-titanium alloys are widely used in the aviation industry as large-sized structural components with special shapes[1]. This kind of components must meet the strict requirements for mechanical properties. However, the large-sized structural components usually have microstructural heterogeneity, which leads to mechanical behavior anisotropy. For bimodal microstructures of metastable β-titanium alloys, due to the non-uniformity of temperature and strain of large-sized structural components during die forging processes, the volume fraction, size, morphology and microtexture of α phase are different, making it difficult to achieve microstructural homogeneity of alloys after die forging[24–26].

Fig. 2 shows OM images of the Ti55511 component after die forging, in which the white phase is α phase. It can be observed that the grain size of β grain is not uniform, so does the distribution of primary α phase. This is due to different degrees of deformation of grains with different orientations and different internal deformation storage energies. The microstructure differences among local areas are very small.

Fig. 3 shows SEM images of the Ti55511 component after die forging. After die forging, basket-weave microstructure forms mainly in the Ti55511 component. In different grains, the degree of precipitation of primary α phase varies. Different degrees of deformation make the ability of grains to induce precipitation, dynamic globalization and coarsening of α phase. For example, in area 1-1, 1-2 and 1-3, the volume fraction of equiaxed α phase is the lowest, whereas that is the highest in area 2-1 and 2-2. The area 1-1, 1-2 and 1-3 have the least strain during die forging, whereas area 2-1 and 2-2 have the largest strain during die forging.

The formation of basket-weave microstructure in area 1-1, 1-3, 3-2 and 3-3 is due to the high forging temperature above β-transus temperature. During the forging process, very few α phases are precipitated. As a result, α phase is mainly precipitated during the cooling process, and the Burgers relationship can be maintained well. Moreover, the deformation temperature of the first three steps of die forging is about 870 °C, and some equiaxed α phases form through dynamic globalization. However, equiaxed α phases gradually disappear after the last forging step in area 1-1, 1-3, 3-2 and 3-3. It also indicates that the degree of dynamic globalization in these local areas in the early stage is low, otherwise the equiaxed α phase will not dissolve at once.

Fig. 4 shows T-IPF maps of local areas corresponding to Fig.2 and Fig.3. Bimodal structure exists in the area 2-1 which undergoes the largest strain in the separated deformation area as mentioned above. It can be observed that the number of <100> oriented grains is the largest in area 2-1 and 2-2, which undergo the largest strain. The number of DRX β grains in area 2-1 is the largest. Low angle grain boundaries (LAGBs) with misorientations 3°−15° are colored in red, and high angle grain boundaries (HAGBs) with misorientations greater than 15° are in black.

The reconstructed T-IPF maps of β phase are shown in Fig.5, in which HAGBs are set as black. To check the texture characteristics of β phase, the α phase is removed. The microstructures of local areas are similar, and the grain shape of β phase is approximately equiaxed, with a certain orientation gradient inside, indicating a state of deformation recovery. The grain size decreases slightly as the strain increases. However, there is a significant difference in orientation. In local area 2-1 with the largest strain, the

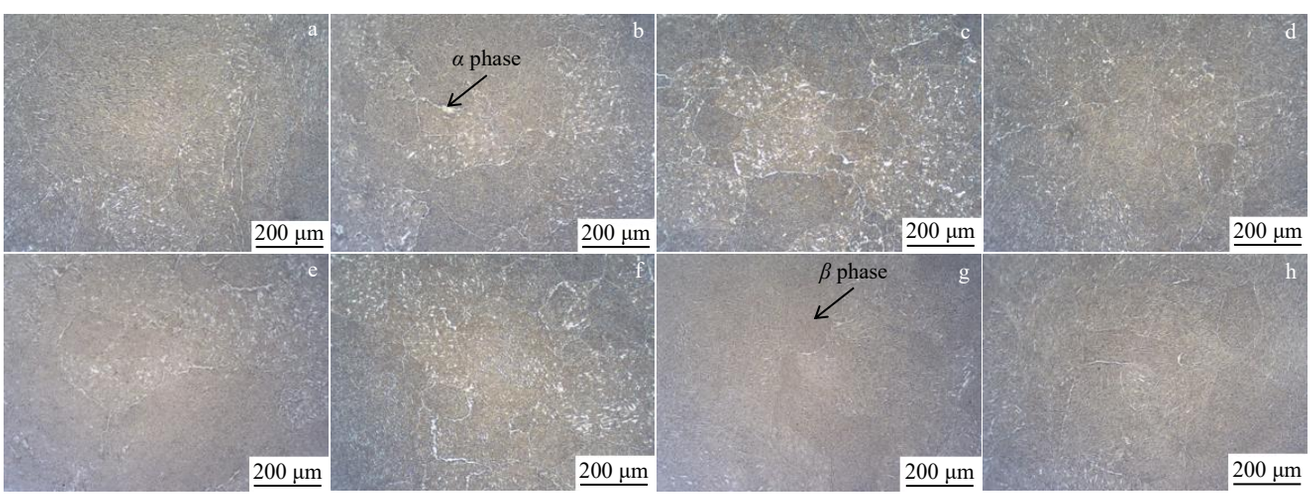

Fig.2 OM images of different local areas in samples after die forging: (a) area 1-1; (b) area 2-2; (c) area 3-1; (d) area 1-2; (e) area 2-1; (f) area 3-2; (g) area 1-3; (h) area 3-3 (the phase with white color is α phase)

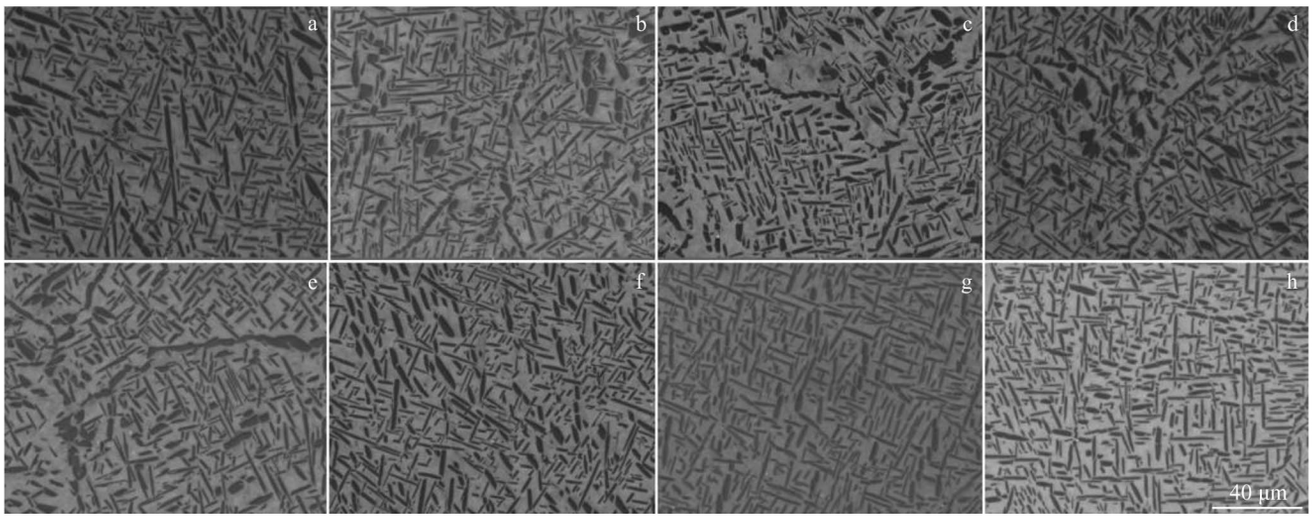

Fig.3 SEM images of different local areas in samples after die forging: (a) area 1-1; (b) area 2-2; (c) area 3-1; (d) area 1-2; (e) area 2-1; (f) area 3-2; (g) area 1-3; (h) area 3-3 (the phase with black color is *α* phase)

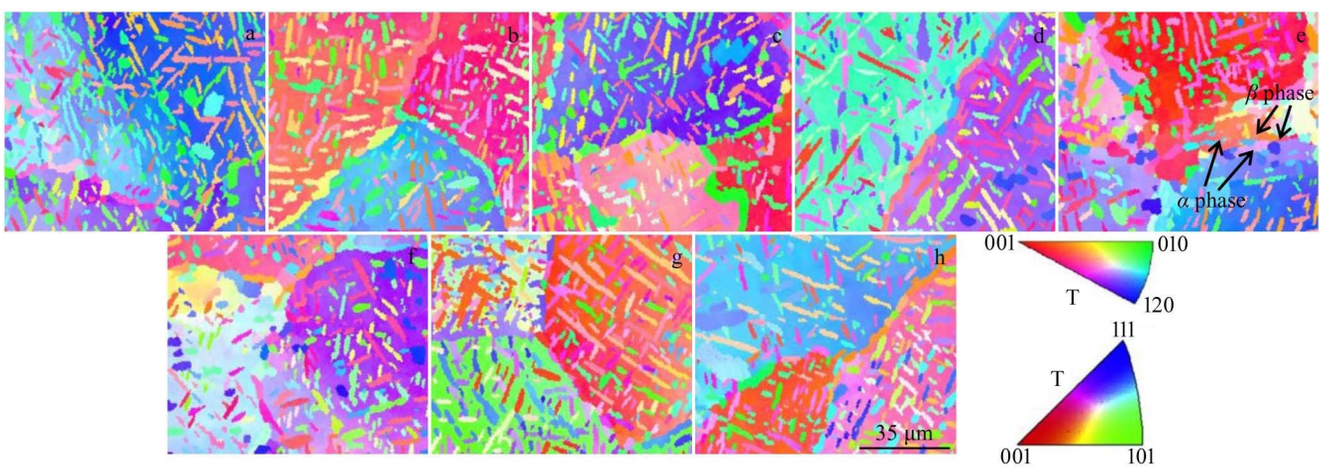

Fig.4 T-IPF maps of different local areas in samples after die forging: (a) area 1-1; (b) area 2-2; (c) area 3-1; (d) area 1-2; (e) area 2-1; (f) area 3-2; (g) area 1-3; (h) area 3-3

number of {100} orientated grains is the largest. In local area 1-1 with moderate strain, there are also some {100} orientated grains. The orientation of local area with 20% strain is the closest to its original orientation.

Fig. 6 shows pole figures extracted from Fig. 5. It can be observed that areas deformed with different degrees exhibit different texture characteristics. No obvious <111> fiber textures form in area 1-1, while some <111>-oriented grains can be observed in Fig.5a. The texture of area 1-3 is relatively random. Overall, local areas with small deformation do not have strong <100> fiber. It is reported that the formation of <100> fiber texture is related to the formation of DRX grains which begins with HAGB bulging[26–27]. Apparently, the microstructures of the areas with small deformation do not have this case. This may be due to the fact that strong <100> fiber texture does not form. There is another possible reason that the strain in this area is not enough to form <100> fiber texture, and there are large grains with nearly <111> orientation (Fig.5a). This may be due to the fact that the area with small deformation during die forging has experienced the same deformation duration as the area with large deformation, so the grains in the area with small deformation have enough time to grow up.

Area 2-2 and 2-1 undergo large deformation during die forging, in which area 2-1 undergo larger deformation than area 2-2. It can be observed that <100>- and <111>-oriented grains are formed in area 2-1. Although there are some <100>-oriented grains, they are not coarse grains. Area 2-2 and 2-1 have larger strain than area 1-1, 1-2 and 1-3 and faster strain rate, but the substructure does not change much. This is due to similar deformation temperature. Unlike the microstructure during hot compression[26–28], the grains in area 2-2 and 2-1 do not become flattened, although this area has undergone the largest strain. It is assumed that DRX occurs during die forging, and the size of <100>-oriented grains is smaller than that of other grains. It is predicted that the <100>-oriented

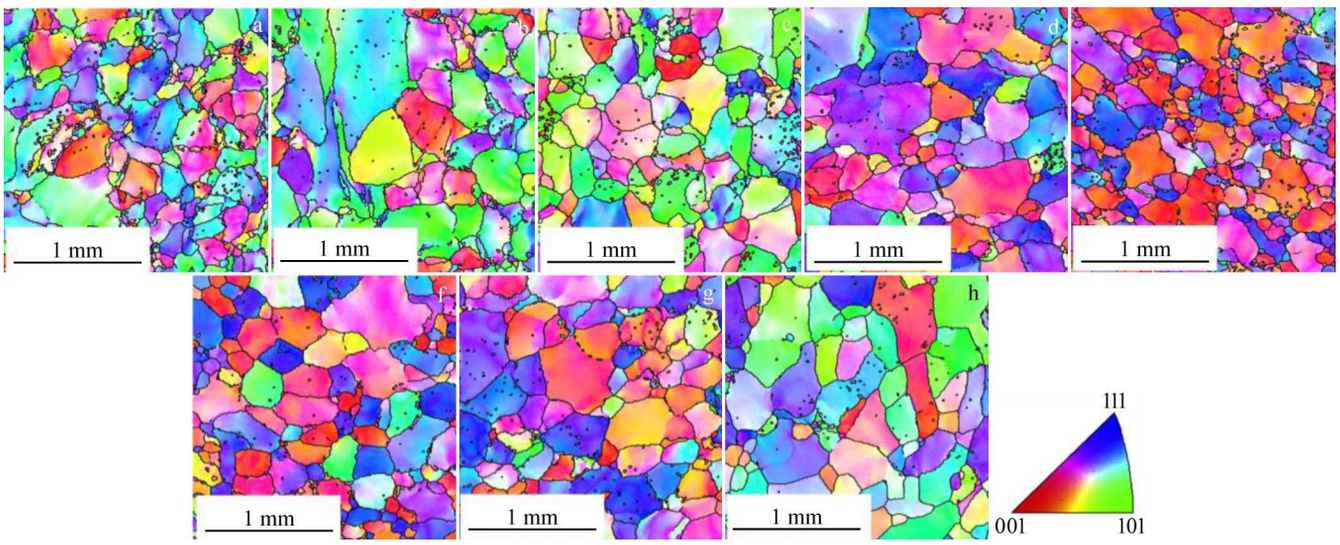

Fig.5 Reconstructed T-IPF maps of different local areas of β phase by removing α phase: (a) area 1-1; (b) area 1-2; (c) area 1-3; (d) area 2-2; (e) area 2-1; (f) area 3-1; (g) area 3-2; (h) area 3-3 (HAGBs are set to black color)

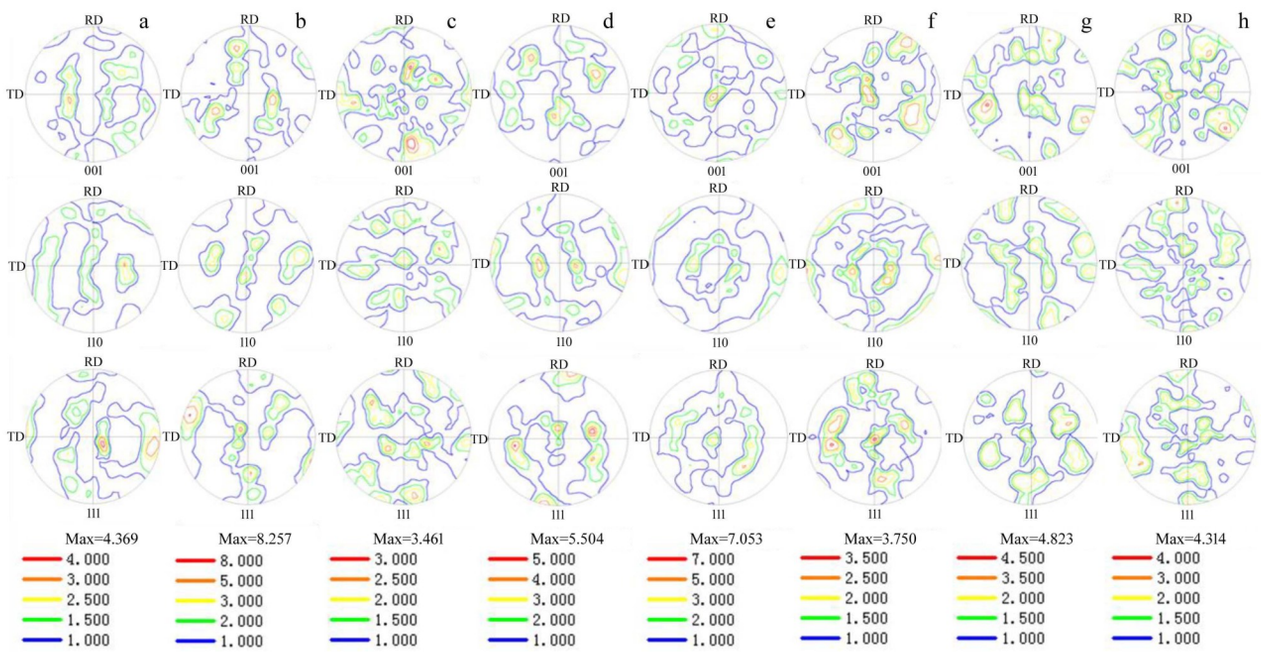

Fig.6 Pole figures of different local areas of samples after die forging extracted from Fig.5: (a) area 1-1; (b) area 1-2; (c) area 1-3; (d) area 2-2; (e) area 2-1; (f) area 3-1; (g) area 3-2; (h) area 3-3

grains are newly formed DRX grains, which are also found in other metastable titanium alloys during hot compression[27]. According to Fig.4, it can be observed that fine DRX β grains are formed with the pinning of equiaxed α grains at the boundaries. The dislocations with high density near equiaxed α grains promote the formation of DRX β grains[31]. In this area, the existing of a large number of α grains contributes to DRX definitely. The texture of area 2-2 becomes weakened because area 2-2 has smaller strain than area 2-1 during hot compression.

Apparently, the favorable texture that is formed by multiple passes of forging in the early stage greatly weakens the strengthening effect of <100> texture during large deformation of die forging.

Area 3-1, 3-2 and 3-3 undergo moderate deformation. Compared with area 2-1, area 3-1 is mainly composed of <111>-oriented grains. The texture characteristic of area 3-2 is similar to that of area 3-1 but the intensity is weakened, maybe because the strain from the center to the edge becomes smaller. Because of the similar texture characteristics and local microstructure, it is considered that the DRX mechanism in area 3-1 is similar to that in area 2-1.

The texture characteristics of these areas after die forgings show that <100>-oriented grains can be easily formed. If a

strong <100> fiber texture is formed in the center of the bar after multiple passes of forging, it can be further strengthened along the hot compression direction, especially during die forging at the high deformation position. This can significantly reduce the mechanical properties of structural components after the die forging[24–25].

Fig. 7 shows HAGBs, LAGBs and DRX grains defined by GOS. Table 1 gives the fraction of GOS grains, HAGBs and LAGBs. It shows that the fraction of HAGBs is higher in the area with higher stain, such as area 1-1, 2-1 and 3-1, and LAGBs have the same trend.

It is found that HAGBs are not bulging, which are serrated in all local areas, so do the LAGBs. The LAGBs are mainly observed in the vicinity of HAGBs, especially in area with smaller strain, such as area 1-1, 1-2, 3-2 and 3-3. And the grain boundaries become more and more serrated with increasing the strain. In the area with higher strain, there are sub-grain structures, such as area 2-1.

DRX grains are small, as shown in black frame area in Fig.7. It should be noted that the small equiaxed black areas in the vicinity of small blue DRX grains are not the unindexed area, which are equiaxed α grains. It can be observed that almost all DRX grains are accompanied with equiaxed α grains. This phenomenon is also observed in local area in Fig. 4. It is considered that the dislocation tangling around equiaxed α grains leads to the formation of DRX β grains[40]. The size of the DRX β grains is about 5 μm, which is similar to the scanning step size of Fig.5. As a result, not all the DRX β grains are indexed in the Fig. 7. It can be seen that in the separated deformation area, the fraction of the DRX grains in area with higher strain is higher than that in area with lower strain.

For the area undergone small deformation, because the strain from the center to the edge becomes smaller, the strain at the area 1-1, 1-2 and 1-3 decreases during deformation (Fig. 1). From Fig. 7, it is found that almost all grain boundaries do not bulge but become serrated, which is because the deformation temperature is near β-transus temperature[26,31].

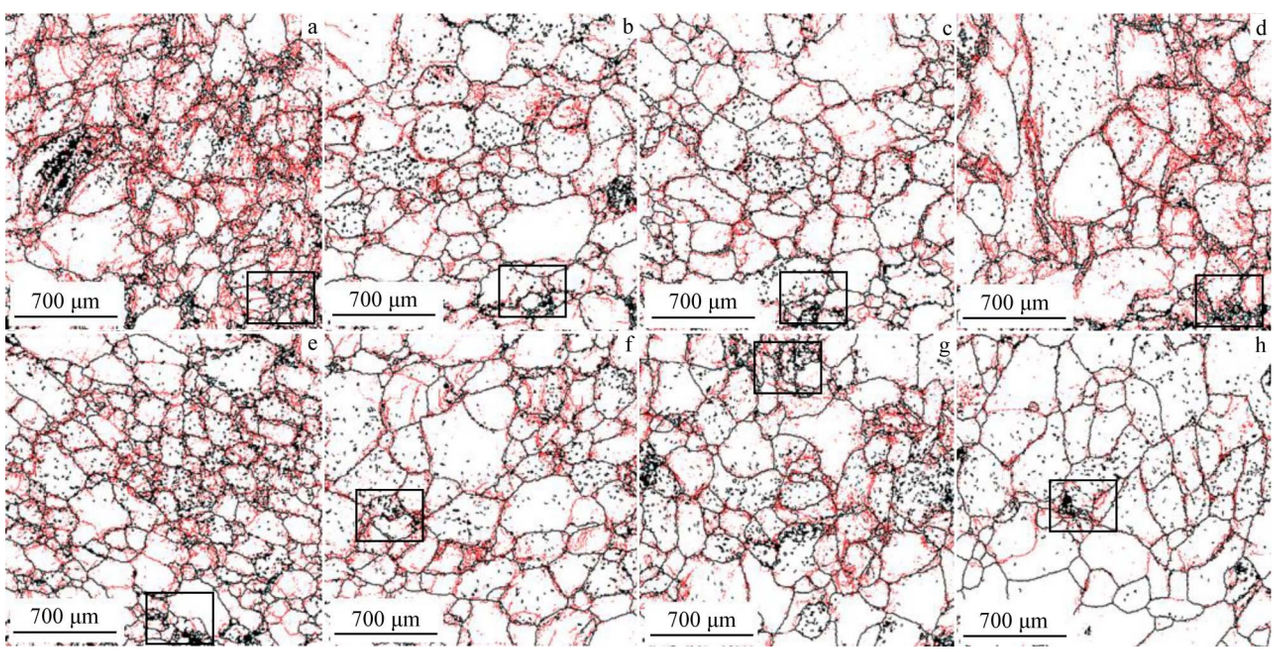

Fig.7 EBSD grain boundary maps of β phase in different areas: (a) area 1-1; (b) area 2-2; (c) area 3-1; (d) area 1-2; (e) area 2-1; (f) area 3-2; (g) area 1-3; (h) area 3-3 (GOS grains are set to blue color, HAGBs are set to black color and LAGBs are set to red color)

Moreover, the sub-grains are not equiaxed and do not coarsen with strain. Apparently, this is not the typical microstructure of dynamics recovery. It is predicted that stored energy cannot cause dislocation climb and cross-slip due to deformation temperature[39].

As shown in Table 2, the average grain size of β phase does not show obvious trend with strain in all areas, while the average grain sizes of β phase decrease with increasing the strain in the separated deformation areas. Fig. 8 shows the grain size distributions. It shows that the grains with small size (<30 μm) have the largest fraction, much higher than fractions of other sizes of grains in all areas. The grain size

Table 1 Fraction of GOS grains, LAGBs and HAGBs

Area	GOS grain	LAGBs	HAGBs
1-1	0.030	0.20	0.08
1-2	0.032	0.16	0.07
1-3	0.015	0.11	0.08
2-1	0.018	0.13	0.08
2-2	0.012	0.11	0.06
3-1	0.015	0.09	0.07
3-2	0.070	0.10	0.06
3-3	0.004	0.06	0.06

Table 2 Average grain size of β phase in different areas

Area	Grain size/μm
1-1	48.38
1-2	62.90
1-3	65.83
2-1	58.40
2-2	78.93
3-1	80.98
3-2	86.17
3-3	97.35

distribution does not show obvious trend with strain. This may be because the grain size is not uniform before die forging.

Kernel average misorientation (KAM) maps are shown in Fig.9. It shows that the grains in area with high strain always keep high dislocation density inside the grains and in the rim of grain boundaries, such as area 2-1, 1-1 and 3-1. In areas with low strain, the dislocation inside grains is obviously higher than that in rim of the grain boundaries.

2.2 Analysis of abnormal growth of grains

Fig.10 shows coarse grain zone in Ti55511 component after die forging. From the low-magnification image of the component (Fig. 10b), coarse grain zone can be observed, as shown in frame area. The coarse grains (about several millimeters, as shown by white arrows in Fig10c) are separated from each other and surrounded by fine grains; the long coarse grains are horizontal, which is consistent with the flow direction of the alloy during compression.

Fig. 11 shows OM and SEM images of abnormal coarse grain zones and fine grain zones. From Fig.11a–11d, it can be

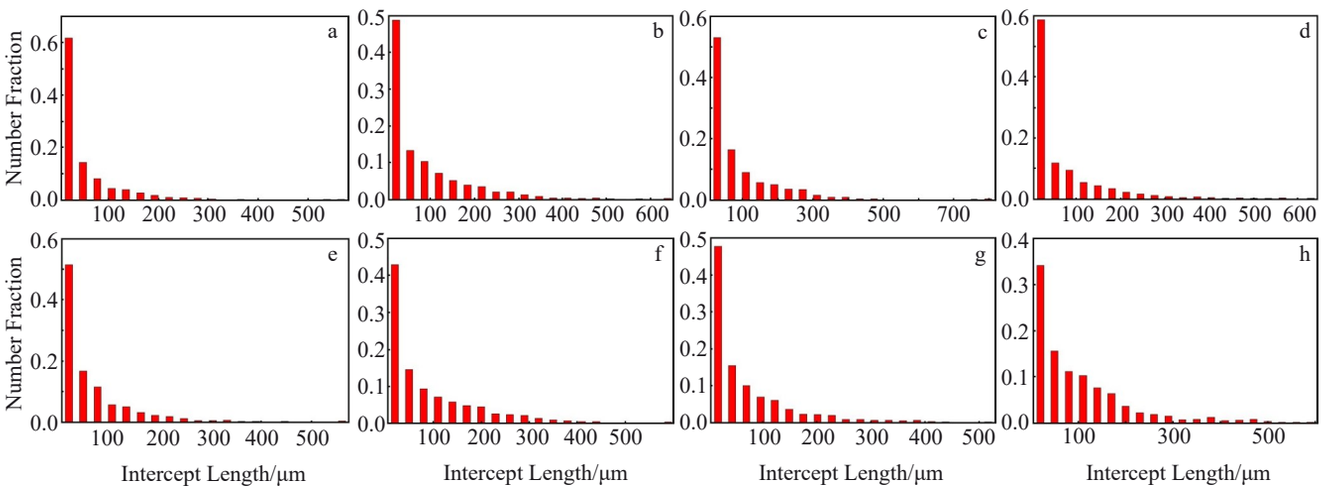

Fig.8 Grain size distributions of β phase in different local areas: (a) area 1-1; (b) area 2-2; (c) area 3-1; (d) area 1-2; (e) area 2-1; (f) area 3-2; (g) area 1-3; (h) area 3-3

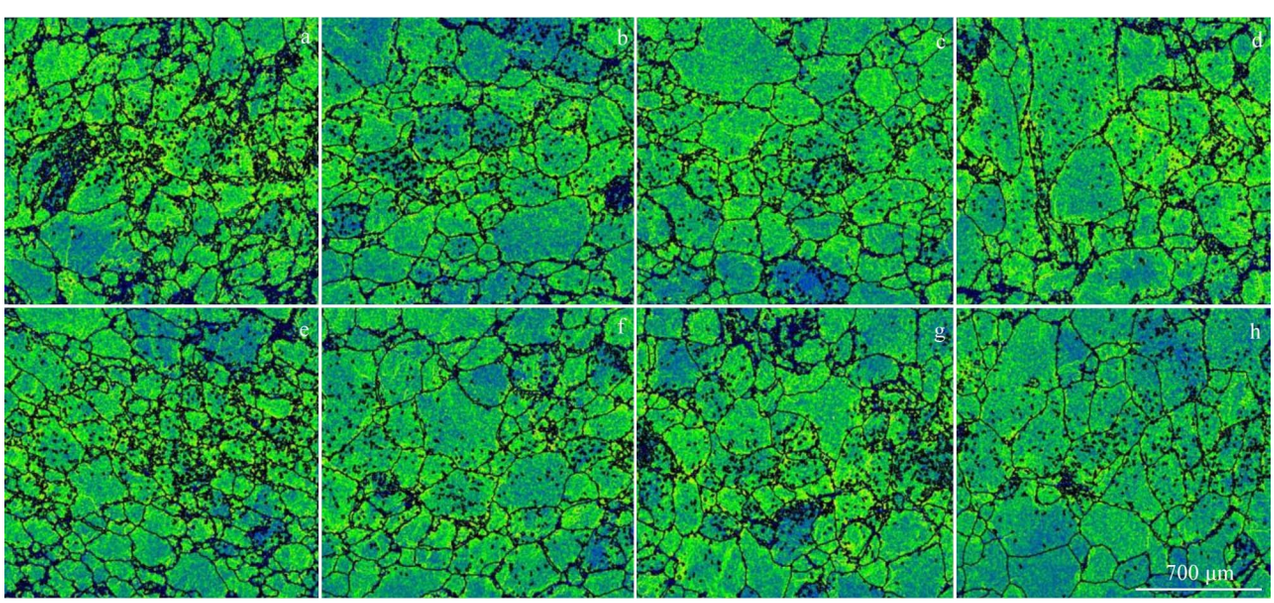

Fig.9 KAM maps of different local areas after die forging: (a) area 1-1; (b) area 2-2; (c) area 3-1; (d) area 1-2; (e) area 2-1; (f) area 3-2; (g) area 1-3; (h) area 3-3

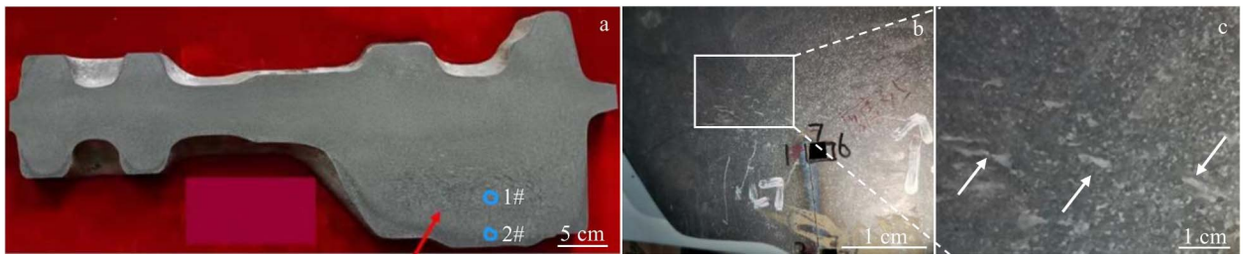

Fig.10 Coarse grain zone in Ti55511 component after die forging (a), local area pointed by red arrows in Fig.10a (b), and local area framed in Fig.10b (c)

observed that grains in the coarse grain zone 1# in Fig.10a is coarse and the grain boundaries are not obvious, whereas the grain boundaries of grains in fine grain zone 2# in Fig.10a are obvious. From SEM images (Fig.11e–11h), the α phase of fine grain zone 2# edge is smaller than that of coarse grain zone 1#. This may be because the edge contacts the die directly during compression, and the cooling rate of the edge is faster than that of the center. It is also found that the arrangement of α plates is relatively consistent, and the type of α variants is few. However, there are more types of α variants in coarse grain zones 1#.

Fig. 12 shows EBSD mappings and corresponding image quality (IQ) maps of abnormal coarse grain zone 1# and surrounding fine grain zone 2#. The grains are in deformed state and there are no grains of static recrystallization.

The individual abnormal coarse grain is shown in Fig. 12a. It is speculated that this large grain is the result of strain-induced grain growth caused by the high temperature during die forging.

The orientation characteristics of fine grains around coarse grains are also measured (Fig. 13). The results show that the orientation of them is random and the microstructure is uniform. The grain size is not much different from that of grains of local areas in Table 2.

Fig. 14 shows EBSD mappings of fine grain zone 2# at the edge of the component. It can be seen that the area has a

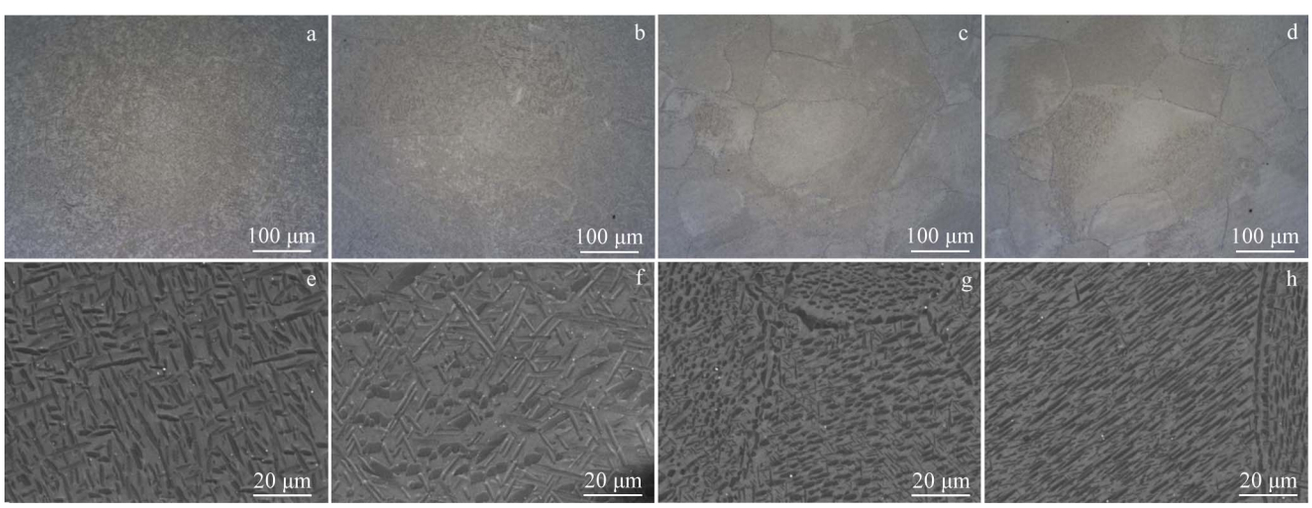

Fig.11 OM (a–d) and SEM (e–h) images of abnormal coarse grain zone 1# (a–b, e–f) and fine grain zone 2# (c–d, g–h) marked in Fig.10a

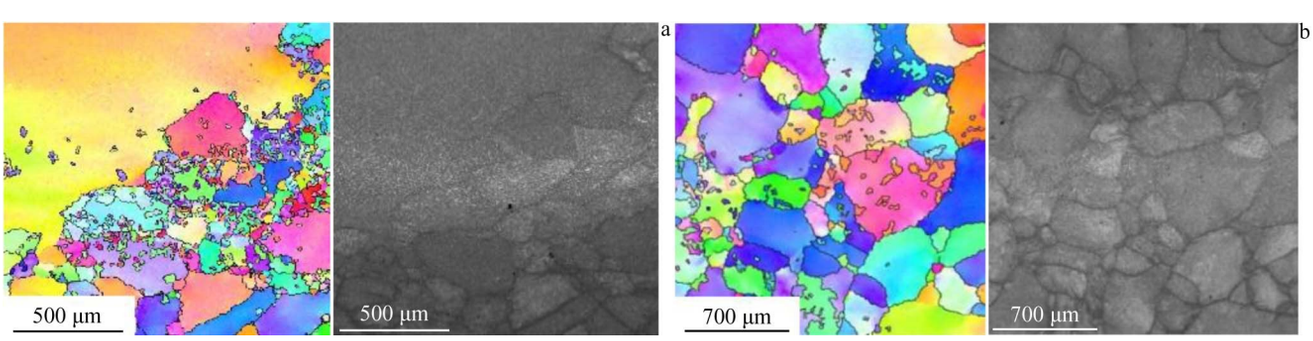

Fig.12 EBSD and corresponding IQ maps of abnormal coarse grain zone 1# (a) and fine grain zone 2# (b)

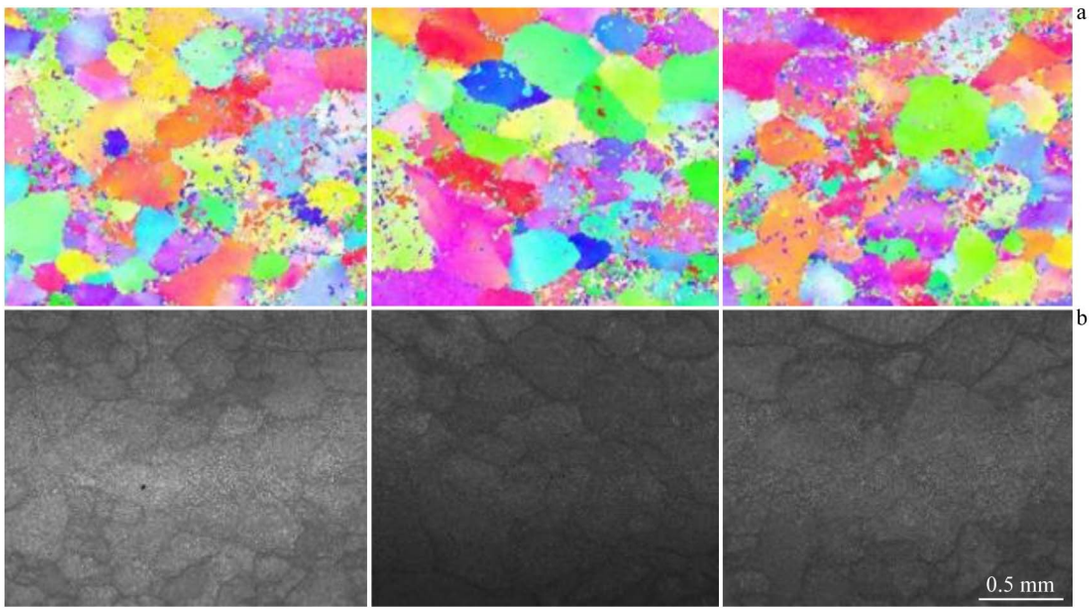

Fig.13 Fine grain zone 2# around coarse grain zone 1# (a) and corresponding IQ mapping (b)

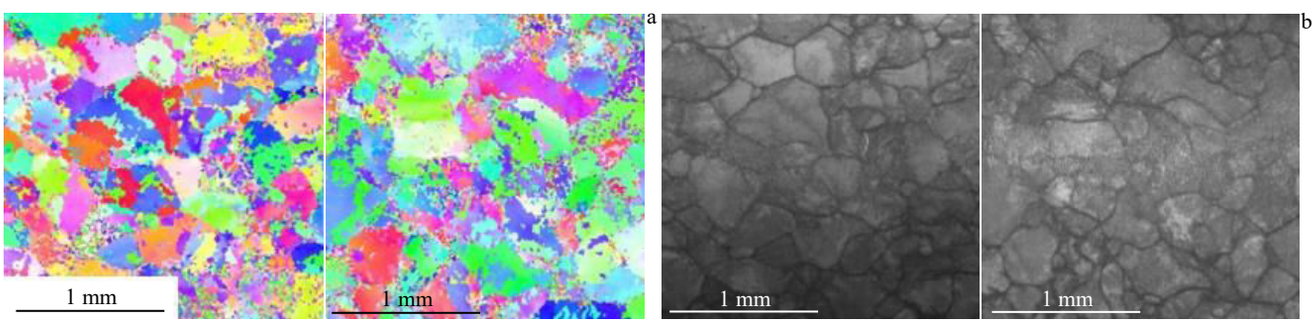

Fig.14 EBSD maps of fine grain zone 2# at the edge of the component (a) and corresponding IQ mapping (b)

greater degree of deformation and more local areas are not indexed. The orientation distribution of this area is random. The grain size is similar to that of the fine grains around coarse grain zone 1#.

3 Conclusions

1) The formation and evolution of texture change with the cumulative strain of metastable β-titanium alloy Ti55511 during the four die forging steps are analyzed. <100>-oriented grains form in the area with the strain of 82.4%, and the original <110>-oriented grains disappear.

2) After die forging, the microstructural characteristic is basket-weave microstructure. Basket-weave microstructure forms due to the dissolution of the α phase. The equiaxed α phase formed in the last forging process disappears.

3) In some small local areas, obvious grain coarsening occurs. The millimeter-sized large grains appear near the edges, which is caused by deformation induction during the last forging process. There are orientation gradients within the overall β phase grains, indicating deformed state of microstructure.

4) From the center to the edge of the component, the orientation rotation at the center is slightly faster than at the edge, so area 1-1, 2-1 and 3-1 have a faster orientation rotation than area 1-3, 2-2 and 3-3.

References

1 Lütjering G, Williams J C. *Titanium Matrix Composites*[M]. Berlin Heidelberg: Springer, 2007: 313

2 Boyer R R, Briggs R D. *Journal of Materials Engineering and Performance*[J], 2005, 14: 681

3 Shi X, Zeng W, Xue S *et al. Journal of Alloys and Compounds*[J], 2015, 631: 340

4 Gu B, Chekhonin P, Schaarschuch R *et al. Journal of Alloys and Compounds*[J], 2020, 825: 154082

5 Huang C, Zhao Y, Xin S *et al. International Journal of Fatigue*[J], 2017, 94: 30

6 Jha S K, Ravichandran K S. *JOM*[J], 2000, 52: 30

7 Prakash D G L, Honniball P, Rugg D *et al. Acta Materialia*[J], 2013, 61(9): 3200

8 Zhao Z B, Wang Q J, Hu Q M *et al. Acta Materialia*[J], 2017, 126: 372

9 Glavicic M G, Bartha B B, Jha S K *et al. Materials Science and Engineering A*[J], 2009, 513: 325

10 Lowden M A W, Hutchinson W B. *Metallurgical Transactions A*[J], 1975, 6: 441

11 Germain L, Gey N, Humbert M *et al. Acta Materialia*[J], 2008, 56(16): 4298

12 Semiatin S L. *Metallurgical and Materials Transactions A*[J], 2020, 51(6): 2593

13 Sander B, Raabe D. *Materials Science and Engineering A*[J], 2008, 479(1–2): 236

14 Banerjee D, Williams J C. *Acta Materialia*[J], 2013, 61(3): 844

15 Kolli R P, Devaraj A. *Metals*[J], 2018, 8(7): 506

16 Sauer C, Luetjering G. *Journal of Materials Processing Technology*[J], 2001, 117(3): 311

17 Wang Fuqiang, Zhang Ruixue, Yang Lixin *et al*. *Materials China*[J], 2023, 42(5): 415 (in Chinese)

18 Ren Xiaolong, Chen Yu, Zhang Sheng *et al*. *Titanium Industry Progress*[J], 2024, 41(3): 14 (in Chinese)

19 Gurao N P, Suwas S. *Materials Science and Engineering A*[J], 2009, 504(1–2): 24

20 Banumathy S, Mandal R K, Singh A K. *Journal of Alloys and Compounds*[J], 2010, 500(2): L26

21 Kou H C, Chen Y, Tang B *et al. Journal of Alloys and Compounds*[J], 2014, 603: 23

22 Chen Y, Li J, Tang B *et al. Journal of Alloys and Compounds*[J], 2015, 618: 146

23 Premkumar M, Himabindu V S, Banumathy S *et al. Materials Science and Engineering A*[J], 2012, 552: 15

24 Chen Liquan, Yang Ping, Li Zhishang *et al. Rare Metal Materials and Engineering*[J], 2021, 50(10): 3600 (in Chinese)

25 Li K, Yang P, Sha A *et al. Acta Metallurgica Sinica*[J], 2014, 50(6): 707

26 Li K, Yang P. *Metals*[J], 2017, 7(10): 412

27 Gu B, Chekhonin P, Xin S W *et al. Journal of Alloys and Compounds*[J], 2021, 876: 159938

28 Zhang S, Lin Y C, Jiang Y Q *et al. Journal of Alloys and Compounds*[J], 2024, 987: 174191

29 Pang G D, Lin Y C, Jiang Y Q *et al. Materials Characterization*[J], 2020, 167: 110471

30 Lin Y C, Huang J, He D G *et al. Journal of Alloys and Compounds*[J], 2019, 471

31 Gu B, Chekhonin P, Xin S W *et al. Materials Characterization*[J], 2021, 179: 111297

32 McQueen H J. *Materials Science and Engineering A*[J], 2004, 387: 203

33 Sakai T, Belyakov A, Kaibyshev R *et al. Progress in Materials Science*[J], 2014, 60: 130

34 Cram D G, Zurob H S, Brechet Y J M *et al. Acta Materialia*[J], 2009, 57(17): 5218

35 Hasegawa M, Yamamoto M, Fukutomi H. *Acta Materialia*[J], 2003, 51(13): 3939

36 Wright S I, Nowell M M, Field D P. *Microscopy and Microanalysis*[J], 2011, 17(3): 316

37 Gazder A A, Sánchez-Araiza M, Jonas J J *et al. Acta Materialia*[J], 2011, 59(12): 4847

38 Yin X Q, Park C H, Li Y F *et al. Journal of Alloys and Compounds*[J], 2017, 693: 426

39 Humphreys F J, Hatherly M. *Recrystallization and Related Annealing Phenomena*[M]. Amsterdam: Elsevier, 2012: 415

40 Dikovits M, Poletti C, Warchomicka F. *Metallurgical and Materials Transactions A*[J], 2014, 45: 1586

亚稳态β钛合金Ti55511模锻过程中显微组织演变与变形行为

谷　宾[1]，熊智豪[1]，杨　平[1]，顾新福[1]，颜孟奇[2]，沙爱学[2]

(1. 北京科技大学 材料科学与工程学院，北京 100083)

(2. 中国航发北京航空材料研究院，北京 100095)

摘　要：采用电子背散射衍射法研究了模锻对亚稳态β钛合金Ti55511显微组织演变和变形行为的影响。在模锻之前，对Ti55511合金进行了多道次锻造，以优化钛合金织构导致的力学行为各向异性。结果表明，模锻后，Ti55511部件局部区域表现出不同的显微组织和织构。在所有变形区域都没有发现<100>纤维织构。动态回复再结晶发生在模锻早期承受大应变的区域，大多数局部区域形成了网篮组织。

关键词：亚稳态β钛合金；显微组织；织构；模锻；EBSD

作者简介：谷　宾，女，1987年生，博士，北京科技大学材料科学与工程学院，北京 100083，E-mail：B2200645@ustb.edu.cn